Generalized Model for Photoinduced Surface Structure in Amorphous Thin Films

Chao Lu,[1] Daniel Recht,[2] and Craig Arnold[1,*]

[1]Department of Mechanical and Aerospace Engineering, Princeton University, Princeton, New Jersey 08544, USA
[2]School of Engineering and Applied Sciences, Harvard University, Cambridge, Massachusetts 02138, USA

(Received 22 April 2013; revised manuscript received 2 August 2013; published 5 September 2013)

We present a generalized model to explain the spatial and temporal evolution of photoinduced surface structure in photosensitive amorphous thin films. The model describes these films as an incompressible viscous fluid driven by a photoinduced pressure originating from dipole rearrangement. This derivation requires only the polarizability, viscosity and surface tension of the system. Using values of these physical parameters, we check the validity of the model by fitting to experimental data of As_2S_3 and demonstrating good agreement.

DOI: 10.1103/PhysRevLett.111.105503 PACS numbers: 81.65.−b, 66.30.−h, 68.35.Fx, 78.66.Jg

Introduction.—Photoinduced surface relief structures are generated in a variety of materials including azobenzene-containing polymers, chalcogenide glasses (like As_2S_3, AsSe, and GeAsSe), and other amorphous materials [1–5]. Macroscopic surface structures can be inscribed by illumination with a laser field having spatially varying intensity or polarization [6]. This phenomenon is potentially useful for technologies such as rewritable optical data storage, active optical devices, nanofabrication, and optical actuators [7]. However, to date a complete description of the underlying microscopic mechanism has not been produced.

Much experimental and theoretical work has been performed to clarify the mechanism of this phenomenon. Models have been proposed to describe the formation of surface relief [3,8], where volumetric internal pressure, interaction among dipoles, anisotropic diffusion, or optical gradient forces were considered as the driving force for deformation [9–11]. These efforts have not led to a unified model that captures all experimental observations.

Here we model surface relief formation as arising from viscous flow driven by the opposition of surface tension and an optically induced pressure which provides a driving force for mass transport that depends on both intensity and polarization. Accommodating both of these dependencies in a single model formulation is the main innovation of this work. Simulations using our model agree well with literature data on the temporal and spatial dependence of optically induced surface relief in As_2S_3.

The model.—For simplicity and correspondence with past experiments we model a film of chalcogenide glass exposed to normal-incidence, time-independent, near-band-gap illumination that varies in one direction along its surface (the x axis) but is uniform along the other surface axis (y). At near-band-gap wavelengths films with thicknesses of order 1 micron or less are optically thin and so we take illumination to be uniform in the direction normal to the film's surface (z) [12]. Figure 1 illustrates this coordinate system. We assume that the viscosity remains high enough to justify the low-Reynolds number lubrication approximation to the Navier-Stokes equations [13]. We further posit that surface tension and the optically induced pressure are the dominant forces. The above assumptions bring surface relief formation within the scope of the Navier-Stokes equation simplified into a two-dimensional boundary layer equation in x and z [14] (see Fig. 1).

$$\frac{\partial v_x}{\partial t} + v_x \frac{\partial v_x}{\partial x} + v_z \frac{\partial v_x}{\partial z} = -\frac{1}{\rho}\frac{\partial \mathcal{P}}{\partial x} + \nu \frac{\partial^2 v_x}{\partial z^2} + f, \tag{1}$$

where the v_i's are components of the velocity vector, ρ is the mass density, $\mathcal{P}$ is the total pressure, f is the body force, and ν is the kinematic viscosity. Deriving the standard high-surface-tension lubrication equation in the presence of a pressure and absence of any body force yields

$$\frac{\partial h}{\partial t} \approx \frac{\partial}{\partial x}\left(\frac{h^3}{3\eta}\left[\frac{\partial P(x)}{\partial x} - s\frac{\partial^3 h}{\partial x^3}\right]\right), \tag{2}$$

in which $h(x, t)$ is the film thickness, η is the dynamic viscosity, s is the curvature coefficient of the surface tension, and $P(x)$ is the optically induced pressure, which is assumed to vary only in x because that is the only

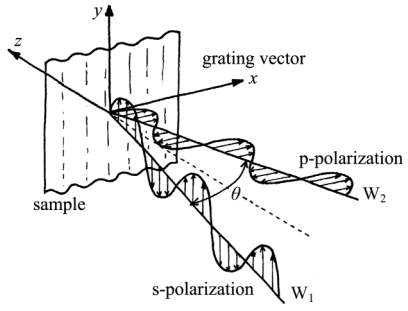

FIG. 1. Schematic of the typical experimental setup used to generate surface structure. Two beams, $W1$ and $W2$, interfere on the surface of a thin film of amorphous, light-sensitive material, leading to the pictured definitions of the coordinate system and polarization directions.

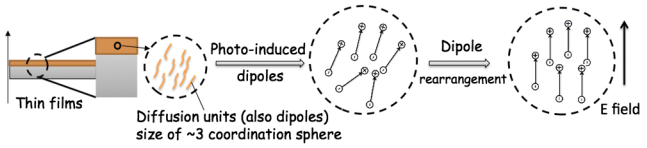

FIG. 2 (color online). Schematic of photoinduced dipoles (on the scale of about 3 coordination spheres [19]) and their rearrangement leading to mass transport [22]. Dipoles can lower their energy by changing configurations in response to the optical electric field. In the case of linear polarization the dipoles will align with the optical electric field.

dimension in which the illumination is modulated [14–17]. The complete derivation can be found in the Appendix. Given a model of the optically induced pressure, Eq. (2) is readily solvable by standard numerical methods.

Our model of the optically induced pressure is based on two assertions. First, the pressure arises from the electric field of the incident light. Second, the material responds through the motion of photoinduced dipoles. In the case of amorphous chalcogenides, each dipole corresponds to a group of atoms on the scale of 3 coordination spheres [18,19] which is capable of rearranging (i.e., mass transport) to change the orientation of the dipole (see Fig. 2). The experimental and theoretical literature indicate that these dipoles persist (fixed to the underlying atomic structure) as long as the illumination is present [19–22]. Moreover, although various mechanisms may generate photoinduced dipoles in different materials [20,23], the model applies as long as those dipoles exist. The strength of the dipoles are given by $\vec{P} = \int d^3 r \rho(\vec{r}) \vec{r}$, where the charge distribution $\rho(\vec{r})$ might be obtained from first-principles calculations [24].

To calculate the photoinduced pressure we start with the relation pressure $\propto \partial$ energy $/ \partial V$. Equations describing the total free energy density of a dipole interaction system in the presence of an electric field are given by Landau [25],

$$\text{energy} = F_0 + \epsilon_{ik} \epsilon_0 E_i E_k, \tag{3}$$

where E_i and E_k are components of the electric field, F_0 is the free energy of the system in the absence of an external field, ϵ_{ik} is a component of the relative permittivity tensor, and Einstein notation has been used. In the dipole interaction model, ϵ_{ik} describes the polarizability of the dipoles when exposed to the optical electric field. Rigorous results for the pressure are obtained from Eq. (3), in terms of the stress tensor

$$\sigma_{ik} = \epsilon_0 E_i D_k. \tag{4}$$

Inserting $D_k = \Sigma(\epsilon_{km} E_m)$ into Eq. (4), yields

$$\sigma_{ik} = \epsilon_0 E_i (\epsilon_{kx} E_x + \epsilon_{ky} E_y + \epsilon_{kz} E_z). \tag{5}$$

Optical electric fields oscillate much faster than any time scale relevant to the flow and so the material must respond to the time average of the electric field. Thus, taking the trace of the stress tensor and calculating its time average, we can write the pressure as

$$\begin{aligned} P &= \frac{1}{3} \langle \mathrm{Tr}(\sigma) \rangle = \frac{1}{3} \langle \sigma_{xx} + \sigma_{yy} + \sigma_{zz} \rangle \\ &= \frac{\epsilon_0}{3} \langle E_x (\epsilon_{xx} E_x + \epsilon_{xy} E_y) + E_y (\epsilon_{yx} E_x + \epsilon_{yy} E_y) \rangle \\ &= \frac{\epsilon_0}{3} \langle \epsilon_{xx} E_x^2 + 2 \epsilon_{xy} E_x E_y + \epsilon_{yy} E_y^2 \rangle. \end{aligned} \tag{6}$$

Noting that the material can respond only to the real part of the electric field, we require $P(E_x, E_y) = P(\tilde{E}_x, \tilde{E}_y)$ where $\tilde{E}_x = \Re\mathrm{e}\{E_x\}$. So Eq. (6) becomes

$$\begin{aligned} P(E_x, E_y) &= P(\tilde{E}_x, \tilde{E}_y) \\ &= \frac{\epsilon_0}{3} \langle \epsilon_{xx} \tilde{E}_x^2 + 2 \epsilon_{xy} \tilde{E}_x \tilde{E}_y + \epsilon_{yy} \tilde{E}_y^2 \rangle. \end{aligned} \tag{7}$$

The coefficients in Eq. (7), which describe the polarizablity of the material, can be measured experimentally [26]. With these coefficients, the pressure is readily calculated. Equation (7), when combined with Eq. (2), completes our model. All the coefficients are determined by the properties of the material. This approach is general for materials that can be thought of as a collection of small, mobile, polarizable units. Furthermore, photoinduced surface relief formation is not observed in most materials because the polarizability of these units is small or because the viscosity and/or surface tension is large.

Simulation.—To check the validity of the model, we calculate the solution to Eq. (2) on a typical holographic setup used to generate surface structure (see Fig. 1). In the setup, everything about the two interfering beams is identical except for the direction of their wave vectors and possibly their polarization. The most generic electric field produced by such interference can then be written

TABLE I. Summary of the photoinduced pressure predicted by Eq. (9) for various polarization conditions. I, ψ, and $\Delta\phi$ are derived from the interference of electromagnetic waves. $\xi = nc\epsilon_0/2$ is a constant. $\delta = \frac{2\pi}{\lambda} x \sin\frac{\theta}{2}$ for θ as in Fig. 1.

Polarization	$I(x)/\xi$	$\psi(x)$	$\Delta\phi(x)$	$P(x)$
s-s	$2E_m^2(x)(1+\cos 2\delta)$	$\pi/2$	0	$(c_1 - c_2) 2E_m^2(x)(1+\cos 2\delta)$
p-p	$2E_m^2(x)(1+\cos 2\delta)$	0	0	$(c_1 + c_2) 2E_m^2(x)(1+\cos 2\delta)$
s-p	$2E_m^2(x)$	$\pi/4$	-2δ	$2E_m^2(x)(c_1 + c_3 \cos 2\delta)$
45–135	$2E_m^2(x)$	δ	$-\pi/2$	$2E_m^2(x)(c_1 + c_2 \cos 2\delta)$
LCP-RCP	$2E_m^2(x)$	δ	0	$2E_m^2(x)(c_1 + \sqrt{c_2^2 + c_3^2} \sin[2\delta + \arctan(c_3/c_2)])$

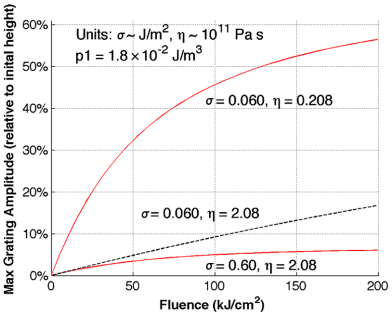

FIG. 3 (color online). Plots of maximum grating amplitude evolution versus irradiation fluence (time). The curve is produced by taking snapshots of the surface profile at different fluence and recording the maximum grating amplitude for each. Each curve corresponds to a set of material parameters: $\{p_1, \sigma, \eta\}$, where p_1 is directly related to the polarizability ϵ_{ij} (see Table I), σ is surface tension, while η is the dynamic viscosity. The upper curve, generated by $\{p_1 = 1.8 \times 10^{-2}\ \mathrm{J/m^3}$, $\sigma = 0.060\ \mathrm{J/m^2}$, $\eta = 0.208 \times 10^{11}\ \mathrm{Pa \cdot s}\}$, simulates the response of As_2S_3.

$$e^{i(kx-\omega t)}\begin{pmatrix} |E_x|e^{i\phi_x} \\ |E_y|e^{i\phi_y} \end{pmatrix}, \tag{8}$$

where $|E_x|$, $|E_y|$, ϕ_x, and ϕ_y are arbitrary, real, and time (but not necessarily position) independent. Defining a generalized polarization angle $\psi = \arctan|E_y|/|E_x|$, inserting E_x and E_y from Eq. (8) into Eq. (7), and computing the time averages gives

$$P = \frac{I(x)}{\xi}[c_1 + c_2 \cos 2\psi(x) + c_3 \cos\Delta\phi(x) \sin 2\psi(x)], \tag{9}$$

where the optical intensity $I(x)/\xi = |E_x(x)|^2 + |E_y(x)|^2$, may vary only along x axis, $\xi = nc\epsilon_0/2$, and the coefficients are: $c_1 = \epsilon_0\epsilon_{xx}/6$, $c_2 = \epsilon_0(\epsilon_{yy} - \epsilon_{xx})/6$ and $c_3 = \epsilon_0\epsilon_{xy}/3$. Equation (9) is intuitively reasonable since it depends on intensity, polarization, and $\Delta\phi$, the three quantities whose modulation has been experimentally shown to cause surface relief formation [3,27]. Taking the first spatial derivative of Eq. (9) yields

$$\begin{aligned}\frac{\partial P}{\partial x} = {} & \frac{1}{\xi}\frac{\partial I(x)}{\partial x}[c_1 + c_2 \cos 2\psi(x) + c_3 \cos\Delta\phi(x) \sin 2\psi(x)] \\ & + \frac{2I(x)}{\xi}\frac{\partial \psi}{\partial x}[-c_2 \sin 2\psi(x) + c_3 \cos\Delta\phi(x) \cos 2\psi(x)] \\ & + \frac{I(x)}{\xi}\frac{\partial \Delta\phi}{\partial x}[-c_3 \sin\Delta\phi(x) \sin 2\psi(x)].\end{aligned} \tag{10}$$

Equation (10) cleanly separates into three independent terms governing the pressure gradient induced by modulation of the intensity, polarization direction, and phase. Accordingly, this model is consistent with the idea suggested by previous experiments that the intensity and phase modulation effects can be saturated without saturating the polarization modulation effect [3,28,29].

Table I lists the pressure functions predicted by Eq. (9) for commonly used polarization conditions. Despite the widely varying initial conditions considered, in the cases studied $P(x)$ can always be represented by the same general form. From the experimental setup, we also have $|E_x(x)|^2 = |E_y(x)|^2 = E_m^2(x)$, where the real electric field amplitude, [rewritten as $E_m(x)$], typically has a Gaussian profile [$E_m^2(x) = E_0^2 e^{-2(x/p_2)^2}$, where E_0 is the maximum electric field]. This allows Eq. (9) to be rexpressed as

$$P(x) = p_1 e^{-2(x/p_2)^2}[p_3 + \cos(p_4 x + p_5)], \tag{11}$$

where the p_i's are parameters set either by the experimental setup or properties of the material. p_4 is fixed as the spatial modulation frequency and p_2 is the beam radius; both are the same across all polarization conditions. p_5 is included to account for the possibility that the Gaussian intensity profile is not centered on a peak of the modulation. p_1 and p_3 are related to the polarizability of the material, which can be measured experimentally [26].

Results.—Figure 3 demonstrates the model's prediction of the dynamics of light-induced grating formation in

TABLE II. Summary of the parameters used in constructing the fit depicted in Fig. 5.

Parameter	Comment	Value
Parameters from experimental setup		
h_0	Initial thickness	2 μm
T	Total illumination time	381 s
p_2	Illumination radius	57 μm
p_3	Nonoscillatory pressure	1
p_4	Modulation frequency	$2\pi/13\ \mu\mathrm{m}^{-1}$
p_5	Modulation phase	$\pi/2$
Fitting parameters by model		
p_1/σ	Relative pressure strength	$0.30\ \mathrm{m}^{-1}$
σ/η	Characteristic growth rate	0.0114 μm/s
Parameters from calculation		
p_1	Extracted from [26] (10^{-2} J/m^2)	0.45–1.8
σ	Surface tension (J/m^2)	0.015–0.060
η	Dynamic viscosity (10^{11} Pa · s)	0.052–0.208

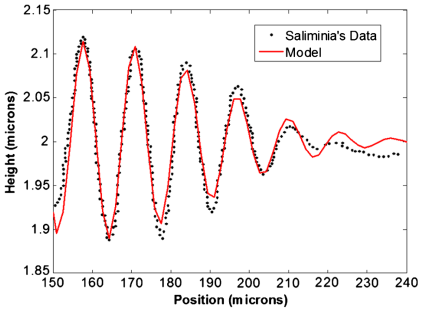

FIG. 4 (color online). The model's fit to a section of a surface relief profile data from [3]. Results by the model agree well with experimental measurements, both in amplitude and frequency.

different hypothetical materials defined by a set of parameters $\{p_1, \sigma, \eta\}$, assuming p-p polarization. The illumination radius p_2 is 57 μm, and the model is evaluated using the finite difference method with a time step of 1/200 s. As can be seen from the figure, lower surface tension and viscosity lead to higher maximum grating amplitude.

In order to test our model we compare it to experimental results for As_2S_3 in [3]. Setting $c_2 = 3c_1$ and $c_3 = 2c_1$ approximates that paper's qualitative description of the observed size ordering for different polarization conditions. This choice captures the well-known anisotropy of As_2S_3 in response to an external optical field and suggests that $\epsilon_{yy} = 4\epsilon_{xx}$ and $\epsilon_{xy} = \epsilon_{xx}$. In order to fit the data, we combine the p_1, η, σ into two ratios, p_1/σ and σ/η and do a least square fit to get the optimal values as given in Table II.

Figures 4 and 5 show the model's fit to the time and space dependence of surface relief formation observed in [3]. The amplitude and frequency of the calculation match the experimental data and growth rate as a function of time fits well over a wide range of fluences.

The values of the fitting parameters can be compared to the literature in order to assess their validity. As described in Eqs. (9)–(11), the polarizabilities ϵ_{ij} are grouped into the parameter p_1 according to the setup geometry. With the values of ϵ_{ij} from [26], p_1 is calculated to be $0.45\text{–}1.8 \times 10^{-2}$ J/m^2. Surface tension and viscosity can then be determined from the values of the fitting parameters, and calculated to be $\sigma = 0.015\text{–}0.060$ J/m^2 and $\eta = 0.052\text{–}0.208 \times 10^{11}$ Pa $\cdot$ s. These agree well with measurements from literature: $\sigma = 0.059\text{–}0.168$ J/m^2 [30], $\eta = 10^{11}\text{–}10^{13}$ Pa $\cdot$ s [31]. Together with Table I, these results explain the intensity and polarization dependence of light-glass interactions in the case where strong relief gratings are observed. The model suggests that not only does intensity modulation lead to grating formation but also cross-polarized holographic exposure of uniform intensity leads to gratings as observed in [3,28].

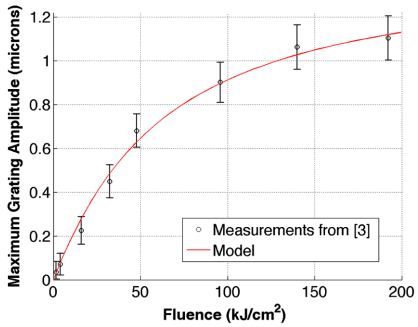

FIG. 5 (color online). Fluence dependence of maximum surface relief amplitude, with measurements data taken from [3].

In summary, the goal of this work was to study the mechanism of photoinduced mass transport and the resulting surface morphology changes in chalcogenide materials, especially As_2S_3. We derived a model based on lubrication theory and an optically induced pressure due to interacting induced dipoles. The model was used to obtain simulation results, which were found to agree well with literature data.

We thank Ashley Prescott for drawing Fig. 1. We gratefully acknowledge support by NSF through the MIRTHE Center (Grant No. EEC-0540832).

Appendix.—To derive Eq. (2) we begin with Eq. (1), in which the v_i's are components of the velocity vector, ρ is the mass density, $\mathcal{P}$ is the total pressure, f is the body force, and ν is the kinematic viscosity. Applying a thin-film approximation sanctions the replacement of $\mathcal{P}$ with its value at the surface since there is little depth over which the pressure can change. At the surface, $\mathcal{P}$ is comprised of surface tension, $\mathcal{S}$, and the photoinduced pressure, P. Surface tension is traditionally taken to be proportional to surface curvature. Symbolically,

$$\mathcal{S} = \sigma \frac{\frac{d^2h}{dx^2}}{[1 + (\frac{dh}{dx})^2]^{3/2}} \approx \sigma \frac{d^2h}{dx^2}, \tag{A1}$$

where h is the (spatially varying) thickness of the film, and the last step is justified by the thin film approximation since this condition implies $dh/dx \ll 1$. We note that since the illumination is modulated only along the x axis, the photoinduced pressure can vary only with x. The thin film approximation thus leads to

$$\mathcal{P} \approx P(x) - \sigma \frac{\partial^2 h}{\partial x^2}. \tag{A2}$$

In addition, we assume there are no body forces so $f = 0$.

Combining this information with Eq. (1) leads to

$$\frac{\partial v_x}{\partial t} + v_x \frac{\partial v_x}{\partial x} + v_z \frac{\partial v_x}{\partial z} = -\frac{1}{\rho} \frac{\partial}{\partial x}\left[P(x) - \sigma \frac{\partial^2 h}{\partial x^2}\right] + \nu \frac{\partial^2 v_x}{\partial z^2}. \tag{A3}$$

Following the analyses of Ledoyen *et al.* and Pimputkar *et al.*, it is possible to drop all the terms on the left-hand side because they turn out to be small in practice [15–17]. Doing so yields

$$\frac{\partial^2 v_x}{\partial z^2} \approx \frac{1}{\eta}\left[\frac{\partial P(x)}{\partial x} - \sigma\frac{\partial^3 h}{\partial x^3}\right], \tag{A4}$$

where $\eta = \rho\nu$ is the dynamic viscosity.

Equation (A4) is solvable subject to the following constraints and boundary conditions. First, we have

$$\frac{\partial v_x}{\partial x} + \frac{\partial v_z}{\partial z} = 0, \tag{A5}$$

which is the continuity equation, derived from incompressibility and conservation of mass. Next, assuming perfect adhesion to the substrate implies

$$v_x = v_z = 0 \quad \text{at} \quad z = 0, \tag{A6}$$

where $z = 0$ is the film-substrate interface. At the free surface of the film, the shear stress along z goes to zero [14,17]. Symbolically,

$$\frac{\partial v_x}{\partial z} = 0 \quad \text{at} \quad z = h. \tag{A7}$$

Finally, the z velocity at the free surface is the rate of change in the height. This can be represented as

$$v_z = \frac{\partial h}{\partial t} \quad \text{at} \quad z = h. \tag{A8}$$

Since the right-hand side of Eq. (A4) has no z dependence, the whole equation can be integrated with respect to z.

$$\frac{\partial v_x}{\partial z} \approx \frac{z}{\eta}\left[\frac{\partial P(x)}{\partial x} - \sigma\frac{\partial^3 h}{\partial x^3}\right] + C_1, \tag{A9}$$

where C_1 is an integration constant. Applying the shear stress boundary condition [Eq. (A7)] yields C_1. Thus,

$$\frac{\partial v_x}{\partial z} \approx \frac{(z-h)}{\eta}\left[\frac{\partial P(x)}{\partial x} - \sigma\frac{\partial^3 h}{\partial x^3}\right]. \tag{A10}$$

Integrating with respect to z again gives

$$v_x \approx \frac{(z^2/2 - hz)}{\eta}\left[\frac{\partial P(x)}{\partial x} - \sigma\frac{\partial^3 h}{\partial x^3}\right] + C_2. \tag{A11}$$

The application of Eq. (A6) shows that C_2 is 0. Taking the derivative of both sides with respect to x and applying the continuity condition of Eq. (A5) yields

$$-\frac{\partial v_z}{\partial z} \approx \frac{\partial}{\partial x}\left(\frac{(z^2/2 - hz)}{\eta}\left[\frac{\partial P(x)}{\partial x} - \sigma\frac{\partial^3 h}{\partial x^3}\right]\right). \tag{A12}$$

This too can be integrated with respect to z.

$$-v_z \approx \frac{\partial}{\partial x}\left(\frac{(z^3/6 - hz^2/2)}{\eta}\left[\frac{\partial P(x)}{\partial x} - \sigma\frac{\partial^3 h}{\partial x^3}\right]\right) + C_3. \tag{A13}$$

Equation (A6) reveals C_3 to be 0 as well.

Finally, setting $z = h$ and applying the last boundary condition [Eq. (A8)] gives

$$\frac{\partial h}{\partial t} \approx \frac{\partial}{\partial x}\left(\frac{h^3}{3\eta}\left[\frac{\partial P(x)}{\partial x} - \sigma\frac{\partial^3 h}{\partial x^3}\right]\right). \tag{A14}$$

*cbarnold@princeton.edu

[1] U. Gertners and J. Teteris, Opt. Mater. **32**, 807 (2010).
[2] Y. Kaganovskii, D. L. Beke, and S. Kokenyesi, Appl. Phys. Lett. **97**, 061906 (2010).
[3] A. Saliminia, T. V. Galstian, and A. Villeneuve, Phys. Rev. Lett. **85**, 4112 (2000).
[4] S. Shtutina, M. Klebanov, V. Lyubin, S. Rosenwaks, and V. Volterra, Thin Solid Films **261**, 263 (1995).
[5] D. Barada, M. Itoh, and T. Yatagai, J. Appl. Phys. **96**, 4204 (2004).
[6] X. L. Jiang, L. Li, J. Kumar, D. Y. Kim, and S. K. Tripathy, Appl. Phys. Lett. **72**, 2502 (1998).
[7] D. Y. Kim, S. K. Tripathy, L. Li, and J. Kumar, Appl. Phys. Lett. **66**, 1166 (1995).
[8] H. Hisakuni and K. Tanaka, Science **270**, 974 (1995).
[9] J. Kumar, L. Li, X. L. Jiang, D. Kim, T. S. Lee, and S. Tripathy, Appl. Phys. Lett. **72**, 2096 (1998).
[10] S. Bian, J. M. Williams, D. Y. Kim, L. Li, S. Balasubramanian, J. Kumar, and S. Tripathy, J. Appl. Phys. **86** 4498 (1999).
[11] P. Lefin, C. Fiorini, and J.-M. Nunzi, Pure Appl. Opt. **7**, 71 (1998).
[12] A. L. Dawar, P. K. Shishodia, G. Chauhan, J. C. Joshi, C. Jagadish, and P. C. Mathur, Appl. Opt. **29** 1971 (1990).
[13] T. G. Myers, SIAM Rev. **40**, 441 (1998).
[14] V. Levich, *Physiochemical Hydrodynamics* (Prentice-Hall, Englewood Cliffs, NJ, 1962), 2nd ed., pp. 372–376 and 669–671.
[15] F. Ledoyen, P. Bouchard, D. Hennequin, and M. Cormier, Phys. Rev. A **41**, 4895 (1990).
[16] S. M. Pimputkar, and S. Ostrach, Phys. Fluids **23**, 1281 (1980).
[17] C. J. Barrett, P. L. Rochon, and A. L. Natansohn, J. Chem. Phys. **109**, 1505 (1998).
[18] H. Fritzsche, Philos. Mag. B **68**, 561 (1993).
[19] J. M. Lee, G. Pfeiffer, M. A. Paesler, D. E. Sayers, and A. Fontaine, J. Non-Cryst. Solids **114**, 52 (1989).
[20] V. K. Tikhomirov and S. R. Elliott, J. Phys. Condens. Matter **7**, 1737 (1995).
[21] V. M. Lyubin and V. K. Tikhomirov, J. Non-Cryst. Solids **164–166**, 1211 (1993).
[22] K. Tanaka, Phys. Rev. B **36**, 9746 (1987).
[23] A. Natansohn, and P. Rochon, Chem. Rev. **102**, 4139 (2002).
[24] T. Uchino, D. C. Clary, and S. R. Elliott, Phys. Rev. B **65**, 174204 (2002).
[25] L. D. Landau and E. M. Lifshitz, *Electrodynamics of Continuous Media* (Pergamon, New York, 1960), p. 58.
[26] J. Perrin, J. Cazaux, and P. Soukiassian, Phys. Status Solidi B **62**, 343 (1974).
[27] K. Tanaka, J. Optoelectron. Adv. Mater. **7**, 2571 (2005).
[28] K. Asatryan, B. Paquet, T. Galstian, and R. Vallée, Phys. Rev. B **67**, 014208 (2003).
[29] K. Asatryan, T. Galstian, and R. Vallée, Phys. Rev. Lett. **94**, 087401 (2005).
[30] T. D. Mel'nichenko, V. I. Fedelesh, T. N. Mel'nichenko, D. S. Sanditov, S. S. Badmaev, and D. G. Damdinov, Glass Physics and Chemistry **35**, 32 (2009).
[31] S. N. Yannopoulos and M. L. Trunov, Phys. Status Solidi B **246**, 1773 (2009).